NIR-Light-Driven Generation of Reactive Oxygen Species Using Ru(II)-Decorated Lipid-Encapsulated Upconverting Nanoparticles

Meijer, M.S.; Saez Talens, V.; Hilbers, M.F.; Kieltyka, R.E.; Brouwer, A.M.; Natile, M.M.; Bonnet, S.A.

LANGMUIR Article
Cite This: Langmuir 2019, 35, 12079−12090
pubs.acs.org/Langmuir

NIR-Light-Driven Generation of Reactive Oxygen Species Using Ru(II)-Decorated Lipid-Encapsulated Upconverting Nanoparticles

Michael S. Meijer,[†] Victorio Saez Talens,[†] Michiel F. Hilbers,[‡] Roxanne E. Kieltyka,[†] Albert M. Brouwer,[‡] Marta M. Natile,*[,§] and Sylvestre Bonnet*[,†]

[†]Leiden Institute of Chemistry, Leiden University, P.O. Box 9502, 2300 RA Leiden, The Netherlands
[‡]Van't Hoff Institute for Molecular Sciences, University of Amsterdam, P.O. Box 94157, 1090 GD Amsterdam, The Netherlands
[§]Institute of Condensed Matter Chemistry and Technologies for Energy (ICMATE), National Research Council (CNR), c/o Department of Chemical Sciences, University of Padova, via F. Marzolo 1, 35131 Padova, Italy

Supporting Information

ABSTRACT: The biological application of ruthenium anticancer prodrugs for photodynamic therapy (PDT) and photoactivated chemotherapy (PACT) is restricted by the need to use poorly penetrating high-energy photons for their activation, i.e., typically blue or green light. Upconverting nanoparticles (UCNPs), which produce high-energy light under near-infrared (NIR) excitation, may solve this issue, provided that the coupling between the UCNP surface and the Ru prodrug is optimized to produce stable nanoconjugates with efficient energy transfer from the UCNP to the ruthenium complex. Herein, we report on the synthesis and photochemistry of the two structurally related ruthenium(II) polypyridyl complexes $[Ru(bpy)_2(\mathbf{5})](PF_6)_2$ ($[\mathbf{1}](PF_6)_2$) and $[Ru(bpy)_2(\mathbf{6})](PF_6)_2$ ($[\mathbf{2}](PF_6)_2$), where bpy = 2,2-bipyridine, **5** is 5,6-bis(dodecyloxy)-2,9-dimethyl-1,10-phenanthroline, and **6** is 5,6-bis(dodecyloxy)-1,10-phenanthroline. $[\mathbf{1}](PF_6)_2$ is photolabile as a result of the steric strain induced by ligand **5**, but the irradiation of $[\mathbf{1}](PF_6)_2$ in solution leads to the nonselective and slow photosubstitution of one of its three ligands, making it a poor PACT compound. On the other hand, $[\mathbf{2}](PF_6)_2$ is an efficient and photostable PDT photosensitizer. The water-dispersible, negatively charged nanoconjugate UCNP@lipid/[**2**] was prepared by the encapsulation of 44 nm diameter $NaYF_4$:Yb^{3+},Tm^{3+} UCNPs in a mixture of 1,2-dioleoyl-*sn*-glycero-3-phosphate and 1,2-dioleoyl-*sn*-glycero-3-phosphocholine phospholipids, cholesterol, and the amphiphilic complex $[\mathbf{2}](PF_6)_2$. A nonradiative energy transfer efficiency of 12% between the Tm^{3+} ions in the UCNP and the Ru^{2+} acceptor $[\mathbf{2}]^{2+}$ was found using time-resolved emission spectroscopy. Under irradiation with NIR light (969 nm), UCNP@lipid/[**2**] was found to produce reactive oxygen species (ROS), as judged by the oxidation of the nonspecific ROS probe 2′,7′-dichlorodihydrofluorescein ($DCFH^{2-}$). Determination of the type of ROS produced was precluded by the negative surface charge of the nanoconjugate, which resulted in the electrostatic repulsion of the more specific but also negatively charged $^1O_2$ probe tetrasodium 9,10-anthracenediyl-bis(methylene)dimalonate (Na_4(ADMBMA)).

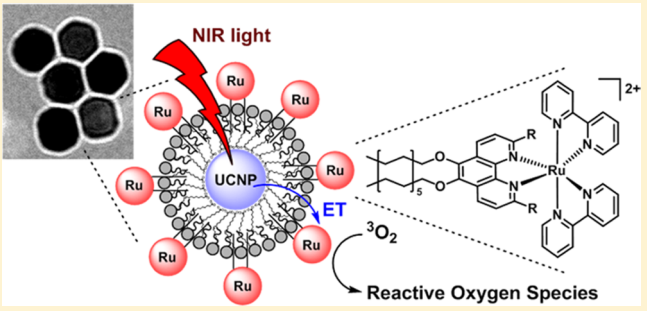

INTRODUCTION

In recent years, the use of light in the treatment of cancer has attracted significant attention, as it can be used to trigger the activation of anticancer prodrugs.[1−5] Phototherapy has the potential to improve the selectivity of chemotherapeutic agents, by providing spatial and temporal control over drug activation. Ruthenium(II) polypyridyl complexes are among the compounds that have proven to be especially suitable for use in phototherapy, both in classical photodynamic therapy (PDT), and in photoactivated chemotherapy (PACT),[6−16] whereas PDT relies on the catalytic light-induced generation of reactive oxygen species (ROS) to kill cancer cells, PACT utilizes the oxygen-independent photodissociation of one of the ligands from the ruthenium center, and thus induce cytotoxicity.[17] Interestingly, small changes to the chemical structure of a ruthenium complex can change it from an efficient photosensitizer for PDT into a photolabile complex with potential use in PACT. A well-known example of this switch in the light-mediated activation mechanism is the introduction of sterically demanding substituents to one or more of the ligands,[18−23] which result in increased strain around the octahedral ruthenium center and a strong decrease in the photostability of the complex, coupled to a dramatic lowering of the singlet oxygen generation quantum yield (Φ_Δ).

Unfortunately, most ruthenium polypyridyl complexes require high-energy visible light (400−500 nm) for their

Received: May 4, 2019
Revised: August 2, 2019
Published: August 7, 2019

photoactivation, which is both harmful to cells[24] and penetrates human tissue poorly.[25] Ideally, one would use light in the "phototherapeutic window" (600−1000 nm) to activate such drugs. This goal can in principle be achieved using upconverting drug delivery systems that generate the desired blue light locally, i.e., inside the tumor, from red or near-infrared light introduced through an external light source, as demonstrated recently by our group using triplet−triplet annihilation upconversion in liposomes.[26]

Another very promising option for upconversion-based drug activation strategies is formed by lanthanoid-doped upconverting nanoparticles (UCNPs), especially as they are insensitive to the presence of molecular oxygen, chemically stable, and show no photobleaching or photoblinking.[27] UCNPs typically consist of $NaYF_4$ nanocrystals doped with Yb^{3+} ions and either Tm^{3+} or Er^{3+} ions, and they are able to produce blue or green light, respectively, under near-infrared (NIR) irradiation at 980 nm, which matches the main absorption peak in Yb^{3+} ions. Over the last 2 decades, UCNPs have been used for a wide range of applications, such as photocatalysis,[28−30] drug delivery,[31] phototherapy,[32−37] bio-imaging and biosensing,[38−40] or security.[41] Nonetheless, the successful application of UCNPs in clinical biology will require the solution of several remaining challenges, such as the high excitation power densities currently required.[27,42] A wide range of examples have been described where PDT photosensitizers are activated using NIR light and UCNPs.[43,44] In most cases, however, green- or red-light-absorbing PDT dyes are employed, e.g., chlorin-e6, zinc phthalocyanine, or rose bengal, combined with the green and red emission of Er-doped UCNPs.[45−47] Although some Tm-doped UCNP-PDT systems have been reported, e.g., using riboflavin or fullerenes as the photosensitizer,[48,49] to the best of our knowledge, no metal-based PDT photosensitizers have been used in combination with UCNPs. On the other hand, some groups have recently shown that ligand-photodissociation reactions in ruthenium polypyridyl complexes can be triggered by a combination of UCNPs and 980 nm light, thus providing an important proof of concept for UCNP-mediated PACT.[35,50−54]

Several strategies have been reported for the conjugation of PDT photosensitizers or PACT prodrugs to the UCNP surface to form a single, water-dispersible drug delivery system. Ideally, we would like to develop a conjugation strategy that is equally suited for use with ruthenium-based PDT and PACT complexes. Embedding the complex into a polymer surface coating, as often done for PDT photosensitizers, can hamper the efficient photorelease of a PACT drug, whereas covalent binding of the complex to the UCNP surface often requires extensive synthetic modifications to the photoactivatable complex. Therefore, the UCNPs were encapsulated in an amphiphilic bilayer, using the already existing oleate layer as the inner leaflet.[55,56] Besides providing a hydrophilic surface coating and increasing the biocompatibility, phospholipid bilayers have been shown to provide ample opportunities for the decoration of the UCNP surface with photoactivatable payloads.[57−59] Furthermore, the group of Capobianco recently showed that the use of negatively charged 1,2-dioleoyl-*sn*-glycero-3-phosphate (DOPA) as the main component of the lipid coating can eliminate the need for the use of bulky PEGylated phospholipids (PEG = poly(ethylene glycol)), which was previously needed to provide colloidal stability, but turned out to be detrimental to the efficient release of a photoactivated payload.[56]

The first example of the application of lipid-coated UCNPs for the activation of metal-based PACT prodrugs was provided by Salassa et al., who successfully activated a Pt(IV) complex situated at the end of a PEGylated phospholipid using NIR light and Tm-doped UCNPs.[57] Here, we designed amphiphilic ruthenium complexes that locate directly at the water−lipid interface of the lipid bilayer, no more than 5 nm from the UCNP surface. With such short distances, the likelihood of efficient nonradiative energy transfer, e.g., Förster resonance energy transfer (FRET) from the upconverting thulium donors to the ruthenium acceptor, should be high enough to lead to activation of either a PDT or a PACT ruthenium compound.[60]

The ruthenium complexes investigated here were based on the well-known photosensitizer $[Ru(bpy)_3]^{2+}$ and its photolabile strained PACT analogue $[Ru(bpy)_2(dmbpy)]^{2+}$, where bpy = 2,2′-bipyridine and dmbpy = 6,6′-dimethyl-2,2′-bipyridine.[22,61] Amphiphilic derivatives of these complexes were designed by the addition of two apolar alkyl tails to the rear of one ligand. Foreseeing that modification of the 1,10-phenanthroline (phen) ligand would be synthetically more accessible than that of bpy, we synthesized the amphiphilic ruthenium(II) polypyridyl complexes $[Ru(bpy)_2(\mathbf{5})](PF_6)_2$, $[\mathbf{1}](PF_6)_2$ and $[Ru(bpy)_2(\mathbf{6})](PF_6)_2$, $[\mathbf{2}](PF_6)_2$ (Scheme 1),

Scheme 1. Schematic Impression of the Nanoconjugate Systems UCNP@lipid/[1] and UCNP@lipid/[2], and the Chemical Structures of $[\mathbf{1}](PF_6)_2$ and $[\mathbf{2}](PF_6)_2$

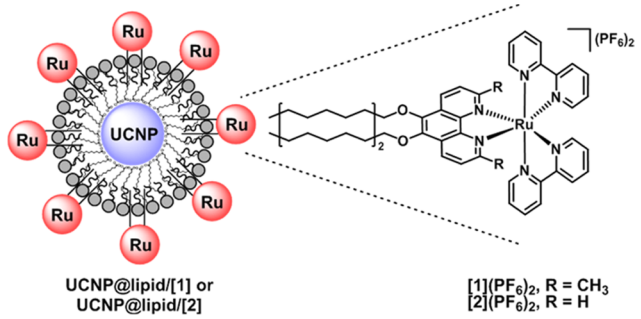

where **5** and **6** are 5,6-dialkylated phen-based ligands. The substitution of the two α-hydrogen atoms of 6 by two methyl groups, renders its ruthenium complex $[\mathbf{1}](PF_6)_2$ sterically strained, lowering its expected photostability, and thus a potential PACT prodrug. On the other hand, the nonstrained complex $[\mathbf{2}](PF_6)_2$ should be a photostable PDT photosensitizer capable of $^1O_2$ generation. We report on the synthesis and photochemistry of the complexes $[\mathbf{1}](PF_6)_2$ and $[\mathbf{2}](PF_6)_2$, the synthesis and upconversion quantum yield measurement of $NaYF_4$:Yb^{3+},Tm^{3+} UCNPs, and the preparation of the ruthenium-decorated, phospholipid-coated UCNP nanoconjugate, UCNP@lipid/[2] (Scheme 1). Using a selection of chemical ROS probes, the generation of reactive oxygen species by UCNP@lipid/[2] was evaluated. Furthermore, we examined the (nonradiative) energy transfer from the UCNP to the ruthenium complex.

RESULTS AND DISCUSSION

Synthesis and Characterization of Upconverting Nanoparticles. Monodisperse UCNPs, consisting of hexagonal phase β-$NaYF_4$, doped with Yb^{3+} (18%) and Tm^{3+} (0.3%) ions, were prepared from a chloride precursor salt, following a modified procedure of Liu et al. (Scheme S3 in the

DOI: 10.1021/acs.langmuir.9b01318
Langmuir 2019, 35, 12079−12090

Supporting Information (SI)).[62] After work-up, the dopant concentration was determined by inductively coupled plasma atomic emission spectroscopy (ICP-OES) (see the SI). The UCNPs were found to be shaped as hexagonal prisms by transmission electron microscopy (TEM), measuring 44 ± 2 nm in diameter (Figure 1A,B), and they were of pure

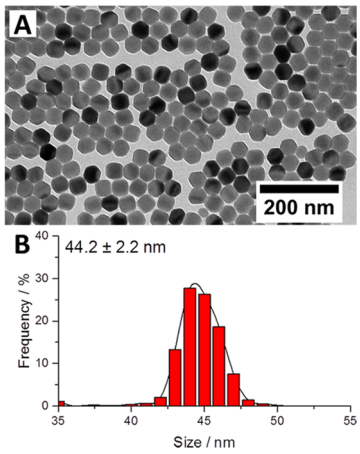

Figure 1. (A) Transmission electron micrograph of the prepared UCNPs. (B) Histograms of the particle size distribution of the nanoparticle sample, as determined by TEM.

hexagonal (β) phase, according to powder X-ray diffraction (XRD, Figure S1). Thermogravimetric analysis (TGA, Figure S2) was employed to calculate the extent of the oleate surface coating. Assuming that each oleate ion covers 0.4 nm^2 of the nanoparticle surface,[63] the 6.3% of organic matter found in the UCNP sample corresponds to an oleate surface coverage of roughly two monolayers.

Excitation of a toluene dispersion of the synthesized UCNPs with 969 nm light resulted in the blue upconverted emission shown in Figure 2D. The emission spectrum (Figure 2A) shows 4f–4f emission bands typical for Tm^{3+}-doped UCNPs (Figure 2B), with emission bands centered at 451 nm ($^1D_2 \rightarrow {}^3F_4$), 475 nm ($^1G_4 \rightarrow {}^3H_6$), 510 nm ($^1D_2 \rightarrow {}^3H_5$), 648 nm ($^1G_4 \rightarrow {}^3F_4$), 698 and 740 nm ($^3F_{2,3} \rightarrow {}^3H_6$), and 803 nm ($^1G_4 \rightarrow {}^3H_5$ and $^3H_4 \rightarrow {}^3H_6$). The multiphotonic nature of the upconversion process is obvious from the excitation power dependence of the individual emission lines, shown in Figure S3. As the so-called slope factor n is larger than one for all power densities, none of the excited states of the thulium manifold is fully saturated under these conditions.[64,65]

Using an absolute method described by us recently,[66] the upconversion quantum yields (Φ_{UC}) of the individual emission bands of these UCNPs in toluene dispersion could be determined (Figures 2C and S4). At the maximum excitation power density used here (50 W cm^{-2}), the total upconversion quantum yield ($\Phi_{UC,total}$) was found to be 0.044 ± 0.006. However, 95% of the observed emission under these conditions is emitted in the form of NIR light of around 803 nm ($\Phi_{UC,803}$ = 0.042 ± 0.006). The desired blue emission of the UCNPs, i.e., the light necessary to activate ruthenium complexes $[\mathbf{1}](PF_6)_2$ and $[\mathbf{2}](PF_6)_2$, is more than 1 order of magnitude weaker, with quantum yields for these two emission bands around 451 and 475 nm of 8.5 ± 1.2 × 10^{-4} and 1.0 ± 0.1 × 10^{-3}, respectively. Quantum yield values for all emission bands are reported in Table S1.

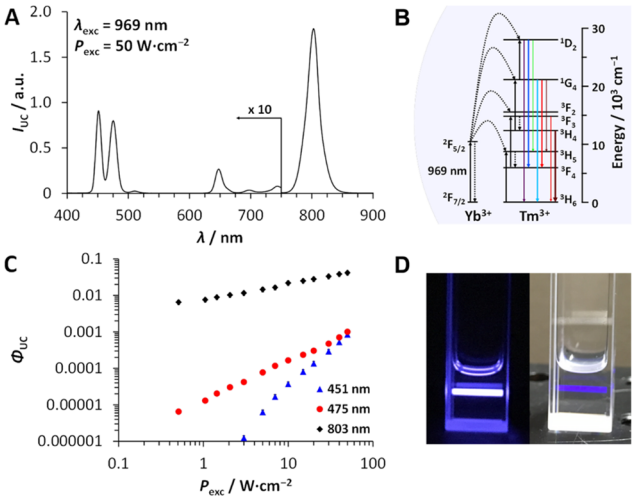

Figure 2. (A) Upconverted emission spectra of UCNPs under 969 nm excitation in toluene (P_{exc} = 50 W cm^{-2}, T = 298 K, [UCNP] = 1 mg mL^{-1}). (B) Simplified energy level diagram depicting the energy transfer upconversion mechanism in the $NaYF_4$:Yb^{3+},Tm^{3+} UCNPs for excitation under 969 nm light, and the assignment of the thulium emission lines. (C) Excitation power dependence of the upconversion quantum yield (Φ_{UC}) of the major emission bands in the $NaYF_4$:Yb^{3+},Tm^{3+} UCNPs in toluene (λ_{exc} = 969 nm, T = 298 K, [UCNP] ≈ 40 mg mL^{-1}, P_{exc} = 0.5–50 W cm^{-2}). (D) Photographs of the upconverted emission under 969 nm excitation in toluene (P_{exc} = 50 W cm^{-2}).

Synthesis of Ruthenium Complexes. Synthesis of complexes $[\mathbf{1}](PF_6)_2$ and $[\mathbf{2}](PF_6)_2$ was performed following a three-step route (Scheme 2). First, commercial 2,9-dimethyl-1,10-phenanthroline and phen were oxidized under relatively mild conditions, as reported by Zheng et al.,[67] to yield their respective 5,6-dione derivatives **3** and **4**. The diketones **3** and **4** were converted into bis-alkylated ligands **5** and **6**, respectively, in a one-pot procedure under basic conditions, involving the reduction of the diketones using sodium thionite, followed by the reaction of the resulting alkoxides with 1-bromododecane.

Coordination of **6** to ruthenium was achieved under reflux in a mixture of ethanol and water, yielding $[\mathbf{2}](PF_6)_2$ after anion exchange in 20% overall yield over three steps. However, the coordination of the sterically demanding ligand **5** to produce $[\mathbf{1}](PF_6)_2$ required the use of solvothermal conditions, i.e., a harsher reaction in ethylene glycol at 200 °C, as described earlier for similar strained ruthenium complexes.[22] Complex $[\mathbf{1}](PF_6)_2$ was finally obtained in 25% overall yield over three steps. The number of signals observed by ^{1}H NMR spectroscopy for the phenanthroline-derived ligands of $[\mathbf{1}]^{2+}$ and $[\mathbf{2}]^{2+}$ indicated that these complex cations are C_2 symmetric in solution. Elemental analysis confirmed that $[\mathbf{1}](PF_6)_2$ and $[\mathbf{2}](PF_6)_2$ were isolated as their bis-hexafluoridophosphate salt. Both complexes were also characterized using high-resolution mass spectrometry and UV–vis absorption spectroscopy (see the Supporting Information).

Photochemistry of $[\mathbf{1}](PF_6)_2$ and $[\mathbf{2}](PF_6)_2$. Since complexes $[\mathbf{1}](PF_6)_2$ and $[\mathbf{2}](PF_6)_2$ were found to be poorly soluble in water, most of their photochemistry was studied in a mixture of acetone and water (1:1 v/v). In this solvent mixture, they formed orange solutions, showing a clear ^{1}MLCT absorption band around 453 nm, independent of the presence of the methyl substituents. The phosphorescence (Φ_P) and singlet oxygen generation quantum yields (Φ_Δ) of $[\mathbf{1}](PF_6)_2$

DOI: 10.1021/acs.langmuir.9b01318
Langmuir 2019, 35, 12079–12090

Scheme 2. Synthesis of Ruthenium Complexes $[1](PF_6)_2$ and $[2](PF_6)_2$[a]

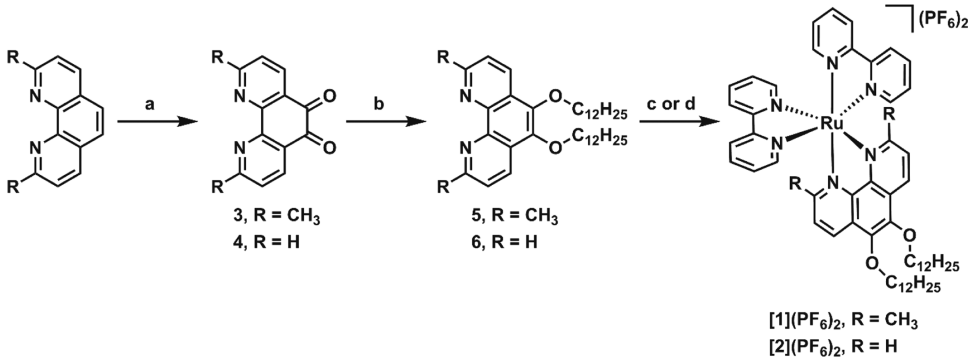

[a]Conditions: (a) $KBrO_3$ in 60% H_2SO_4, room temperature, 24 h, 59% (**3** and **4**); (b) $C_{12}H_{25}Br$, $(n\text{-Bu})_4NBr$, $Na_2S_2O_4$, KOH in tetrahydrofuran/H_2O (1:2), 40 °C, 3 days, 59% (**5**) or 47% (**6**); (c) (i) *cis*-$[Ru(bpy)_2Cl_2]$ in ethylene glycol, solvothermal synthesis, 200 °C, 6 h; (ii) KPF_6, H_2O, 73% ($[1](PF_6)_2$); (d) *cis*-$[Ru(bpy)_2Cl_2]$ in EtOH/H_2O (1:1), reflux, 18 h; (ii) KPF_6, H_2O, 71% ($[2](PF_6)_2$). Compounds $[1](PF_6)_2$ and $[2](PF_6)_2$ were obtained as racemic Λ/Δ-mixtures

Table 1. Lowest-Energy Absorption Maxima (λ_{max}), Molar Absorption Coefficients at λ_{max} (ε_{max}) and 466 nm (ε_{466}), Photosubstitution Quantum Yields (Φ_{466}), and Photosubstitution Reactivities ($\xi_{466} = \Phi_{466} \times \varepsilon_{466}$) at 298 K in Acetone/$H_2O$ (1:1), Singlet Oxygen Quantum Yield (Φ_Δ), and Phosphorescence Quantum Yield (Φ_P) at 293 K in Aerated CD_3OD for Complexes $[1](PF_6)_2$ and $[2](PF_6)_2$

complex	λ_{max}/nm (ε_{max}/M^{-1} cm^{-1})	ε_{466}/M^{-1} cm^{-1}	Φ_{466}	ξ_{466}	Φ_Δ	Φ_P (λ_{em}/nm)
$[1](PF_6)_2$	453 (1.28×10^4)	1.11×10^4	3.5×10^{-4}[a]	3.9[a]	0.005	1.0×10^{-4} (616)
$[2](PF_6)_2$	453 (1.53×10^4)	1.34×10^4			0.73	0.015 (613)

[a]Based on the consumption of $[1](PF_6)_2$, including both possible photosubstitution reactions (substitution of **5** or bpy; see Scheme 3).

and $[2](PF_6)_2$ were determined in aerated CD_3OD solution (Table 1 and Figure S5), whereas $[1](PF_6)_2$ was found to be only very weakly emissive and produced almost no singlet oxygen, $[2](PF_6)_2$ was shown to be a very efficient photosensitizer, with a Φ_Δ value of 0.73, and a phosphorescence efficiency close to that of $[Ru(bpy)_3]^{2+}$ (Φ_P = 0.015).

Both complexes were found to be stable in acetone/H_2O solution in the absence of light (Figure S6A,B). Furthermore, the absorption spectrum of the unstrained complex $[2](PF_6)_2$ did not show any changes upon irradiation with a blue light-emitting diode (LED) (λ = 466 nm, Figure S6C) for 2 h, confirming that this complex is photostable. However, irradiation of a solution of the sterically strained complex $[1](PF_6)_2$ in acetone/water under the same conditions caused a slow bathochromic shift in the absorption maximum from 453 to 481 nm, accompanied by an isosbestic point at 479 nm (Figure 3). Mass spectrometry, performed after 100 min of irradiation (Figure S7), showed the formation of not two, but four photoproducts, identified as $\{bpy + H\}^+$ (m/z = 157.2, calcd m/z = 157.1), $[Ru(bpy)_2(CH_3CN)_2]^{2+}$ (m/z = 247.6, calcd m/z = 248.0), $[Ru(bpy)(\mathbf{5})(CH_3CN)_2]^{2+}$ (m/z = 458.3, calcd m/z = 458.2), and $\{\mathbf{5} + H\}^+$ (m/z = 577.7, calcd m/z = 577.5), as well as the presence of some remaining starting material, i.e., $[\mathbf{1}]^{2+}$ (m/z = 495.0, calcd m/z = 495.3). The acetonitrile ligands stem from the mass spectrometry eluent, as no acetonitrile was used during irradiation. The detected photoproducts indicate the occurrence of two parallel photoreactions, namely, the expulsion of either ligand **5** (Scheme 3, pathway A) or one of the two bpy ligands (Scheme 3, pathway B). Despite the occurrence of two photoreactions, the UV−vis absorption spectra in Figure 3 share an isosbestic point at 479 nm, most likely caused by a strong similarity between the absorption spectra of *cis*-$[Ru(bpy)_2(H_2O)_2](PF_6)_2$ ($[\mathbf{7}](PF_6)_2$) and *cis*-$[Ru(bpy)(\mathbf{5})(H_2O)_2](PF_6)_2$ ($[\mathbf{8}](PF_6)_2$), and the fact that the two photoreactions occur simultaneously. As the changes to the absorbance at 453 nm fitted well to a monoexponential function, the photodegradation of $[1](PF_6)_2$ was treated as a single-step photochemical reaction, and its apparent photochemical quantum yield (Φ_{466}) was found to be 3.5×10^{-4} (Table 1 and Figure S8), which is 2 orders of magnitude lower than the reported quantum yields for similar complexes that bear sterically demanding bipyridine-based ligands.[68,69]

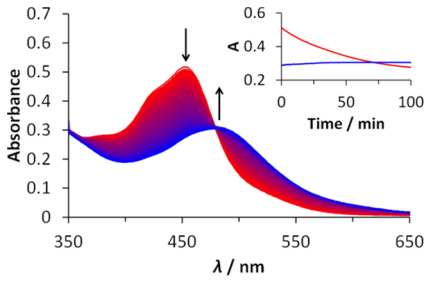

Figure 3. Evolution of the UV−vis absorption spectra of a solution of $[1](PF_6)_2$ (40 μM) in acetone/H_2O (1:1 v/v) upon irradiation (100 min) at 298 K with a 466 nm LED (photon flux $q_p = 1.09 \times 10^{-7}$ mol photons s^{-1}) under N_2. Inset: time evolution of the absorbance at 453 nm (red) and 481 nm (blue) during irradiation.

In the literature, the expulsion of one of the ancillary ligands, as opposed to the straining ligand, has been noted before for ruthenium polypyridyl complexes.[19,70] Already in 1999, the group of Sauvage postulated that the rigidity of the bidentate ligands, i.e., the degree of rotational freedom between the two metal-binding nitrogen atoms, may play a vital role in governing these photoreactions.[19] Here, the irradiation of $[Ru(bpy)_2(dpphen)](PF_6)_2$ (dpphen = 2,9-diphenyl-1,10-phenanthroline) in acetonitrile led to the replacement of one

DOI: 10.1021/acs.langmuir.9b01318
Langmuir 2019, 35, 12079−12090

Scheme 3. Two Photochemical Reactions Observed upon the Visible-Light Irradiation of Complexes $[1](PF_6)_2$ in Acetone/H_2O Solution, Showing (A) Photosubstitution of the Sterically Demanding Bis-methylated Ligand 5, and (B) Photosubstitution of the Ancillary Ligand bpy

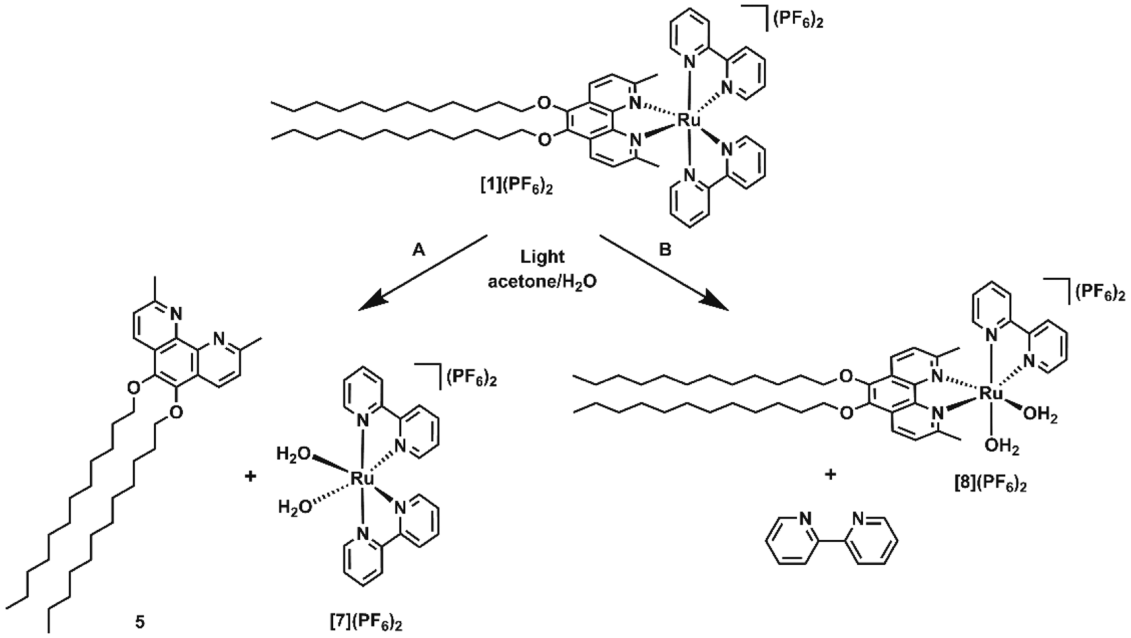

of the bpy ligands rather than the rigid, sterically demanding dpphen ligand. However, the complete loss of selectivity in the photosubstitution reaction seen here for complex $[1](PF_6)_2$, where irradiation leads to the unselective expulsion of one of the three bidentate ligands, is rarely reported.[71] A more thorough investigation into the effect of ligand rigidity on the efficiency and selectivity of such photosubstitution reactions is currently being carried out.

When connected to a nanoparticle surface, the lack of selectivity in the photosubstitution reaction of $[1](PF_6)_2$ impedes the efficient photorelease of ruthenium photoproducts, as product $[8](PF_6)_2$ is likely to remain connected to the UCNP surface. This fact, combined with the very low photochemical quantum yield (Table 1) of $[1](PF_6)_2$, precluded its effective use as a nanoparticle-connected PACT prodrug, so no further studies were undertaken to activate $[1](PF_6)_2$ using UCNPs. On the other hand, the large singlet oxygen generation quantum yield of $[2](PF_6)_2$, combined with its excellent photostability, makes it a good candidate for use as a nanoparticle-bound PDT photosensitizer. Thus, we elected to investigate only the use of $[2](PF_6)_2$ for the decoration of UCNPs.

Synthesis of Lipid-Encapsulated Upconverting Nanoconjugates. As UCNPs are typically obtained with a hydrophobic, oleate surface coating, the introduction of a hydrophilic surface coating is essential for their successful implementation in biological applications. Here, an amphiphilic phospholipid coating is applied to the UCNP surface, forming a supported lipid bilayer that consists of the already present oleate surface coating, and a mixture of DOPA (sodium 1,2-dioleoyl-*sn*-glycero-3-phosphate), cholesterol, and 1,2-dioleoyl-*sn*-glycero-3-phosphocholine (DOPC) in a ratio of 64:7:29. This mixture was recently shown to be effective for the coating of highly faceted $LiYF_4$ UCNPs by Capobianco et al.[56] The phosphate group in the negatively charged DOPA lipid allows this lipid to interact strongly with the lanthanoid ions at the UCNP surface, thereby covering any gaps in the pre-existing oleate coating and providing a negative surface potential to the nanoconjugate. The addition of low quantities of the neutral DOPC lipid prevents electrostatic repulsion between the negatively charged DOPA lipids. Finally, cholesterol is added, as it is known to reduce the water permeability of lipid bilayers by enhancing the tightness of the lipid packing.[72]

Formation of the lipid-coated UCNPs (UCNP@lipid/[**2**]) was performed by a modification of the previously published protocol (Scheme 4).[56] A mixture of phospholipids, cholesterol, $[2](PF_6)_2$, and UCNPs in chloroform was dried to a lipid film. Hydration of this lipid film was performed using a MES/acetate buffer (MES = 2-(*N*-morpholino)ethanesulfonic acid, pH = 6.1), yielding a slightly turbid orange dispersion, and followed by extrusion. The use of phosphate buffer was avoided, as phosphate anions are strongly competing UCNP surface ligands, known to be able to cause particle dissolution upon prolonged exposure.[73−75] Incorporation of 5 mol % of $[2](PF_6)_2$ into the lipid mixture was possible without discernible effects on the dispersibility during the lipid coating procedure. At high concentrations of $[2](PF_6)_2$ (≥15 mol %), the freshly hydrated lipid film was found to be unstable, and could not be extruded due to precipitation of the nanoparticles. Thus, the ruthenium content of UCNP@lipid/[**2**] was kept to 5% of the total molar amount of surfactant added.

After extrusion, the UCNP@lipid/[**2**] particles were separated by centrifugation from the undesired liposomes that formed as side-products, whereas the UCNP@lipid/[**2**] sedimented upon centrifugation at 16 000*g*, liposomes only settle down upon ultracentrifugation (~70 000*g*), and could thus be removed by replacement of the supernatant with fresh buffer after centrifugation. Notably, too extensive washing of the lipid-coated UCNPs leads to the removal of the lipid coating, leaving us to search for an optimal number of washing cycles, whereby we ensured complete removal of the excess lipid and $[2]^{2+}$ but preserved the lipid coating on the UCNP surface. To control this process, the lipid coating was visualized

DOI: 10.1021/acs.langmuir.9b01318
Langmuir 2019, 35, 12079−12090

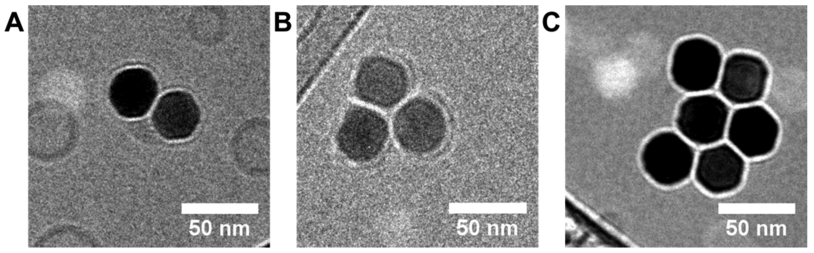

Figure 4. Cryogenic transmission electron micrographs, depicting UCNP@lipid/[**2**] (A) after extrusion, (B) after 1 washing cycle, and (C) after 2 washing cycles. The thickness of the lipid bilayer is 4−5 nm.

Scheme 4. Synthesis of UCNP@lipid/[2] by Phospholipid Encapsulation, Extrusion, and Centrifugal Washing

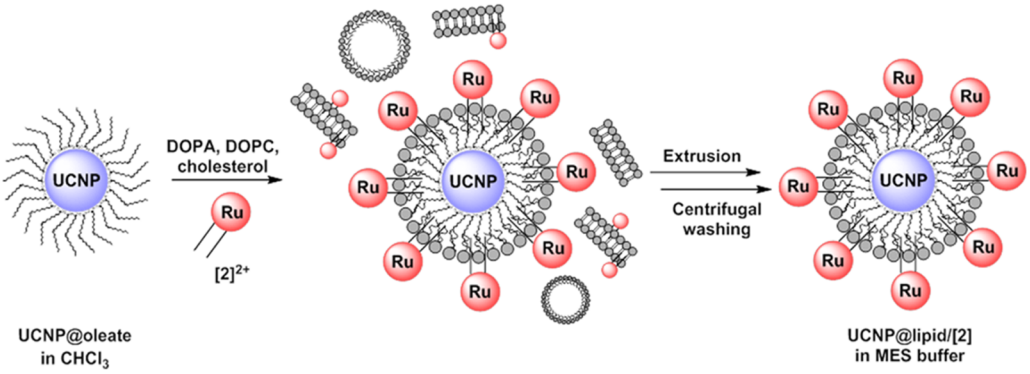

using cryogenic transmission electron microscopy (cryo-TEM, Figures 4 and S9). After extrusion, the presence of liposomes could clearly be observed, as well as the lipid coating, forming a layer on the UCNPs with a thickness of 4−5 nm (Figure 4A), consistent with the typical thickness of a lipid bilayer in liposomes.[72] After the first washing step, this coating layer remained clearly visible, but most of the liposomes had disappeared (Figure 4B). This lipid layer could also clearly be seen using a room-temperature TEM, after the application of uranyl acetate as a negative stain (Figure S10), although the uranyl stain was observed at a larger distance from the UCNP surface (6−14 nm), arguably caused by a remaining excess of lipid. The lighter circular features on these TEM images were identified by us as liposomes, further suggesting the need for a second washing step. After this second washing step, the lipid coating was far less visible on cryo-TEM (Figure 4C) and the white line visible around the particles are more reminiscent of the diffraction fringes that can be seen around uncoated particles (e.g., the UCNP@BF_4 shown in Figure S9D) rather than of lipid coating. However, the remaining presence of the lipid coating was obvious from the strongly negative surface ζ-potential (−60 ± 8 mV, Figure S11B), combined with the clear orange color of the dispersion, even after two washing steps. The UV−vis absorption spectrum of UCNP@lipid/[**2**] (Figure S12) confirmed this visual observation by showing a clear absorption band around 450 nm, reminiscent of the spectrum observed for $[\mathbf{2}]^{2+}$ in acetone/water solution (Figure S6B). This absorption band was not observed for lipid-coated UCNPs without ruthenium addition (UCNP@lipid). These ruthenium-free particles were found to have a similar surface charge (−63 ± 7 mV) to the ruthenium-coated UCNP@lipid/[**2**] (Figure S11B). Dynamic light scattering (DLS) showed that both UCNP@lipid and UCNP@lipid/[**2**] exist in solution as aggregates of several particles, indicated by their hydrodynamic radii of ∼90 and 100 nm, respectively (Figure S11A).

All in all, we found that the use of two washing steps was optimal for the purification of the nanoconjugate, and that the addition of 5 mol % of complex $[\mathbf{2}]^{2+}$ does not significantly affect its size and surface charge, the latter of which is mostly imposed by the negatively charged main lipid component of the bilayer, DOPA.

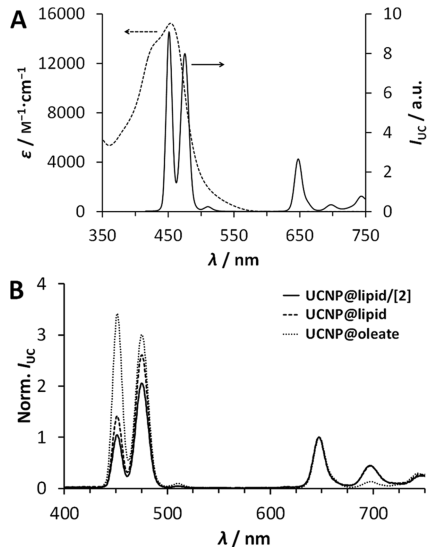

Figure 5. (A) Overlap between the UV−vis absorption spectrum of [**2**]$(PF_6)_2$ in acetone/H_2O (1:1 v/v, dashed line), and the emission of UCNPs in toluene under 969 nm (solid line) excitation. (B) Normalized upconverted emission spectra of UCNP@lipid/[**2**] (solid line) and UCNP@lipid (dashed line) in MES buffer, and oleate-coated UCNPs in toluene (dotted line). Conditions: [UCNP] = 1.0 mg mL^{-1}, T = 298 K, λ_{exc} = 969 nm, P_{exc} = 50 W cm^{-2}, normalized to the emission at 803 nm (not shown).

DOI: 10.1021/acs.langmuir.9b01318
Langmuir 2019, 35, 12079−12090

Figure 5A shows the excellent overlap between the emission of the Tm-doped UCNPs and the absorbance of $[\mathbf{2}](PF_6)_2$. After the coating of $[\mathbf{2}]^{2+}$ onto the surface of the UCNPs, a twenty percent reduction in the blue emission of UCNP@lipid/[2] is observed when compared to the ruthenium-free UCNP@lipid sample (Figure 5B). This reduction suggests that the energy transfer, either radiative or nonradiative in nature, takes place from the UCNP to the ruthenium sensitizer on its surface.

To determine whether the energy transfer from the thulium excited states in the UCNPs to the ruthenium center of $[\mathbf{2}]^{2+}$ was radiative or nonradiative in nature, the time-resolved emission spectra of UCNP@lipid/[2] and UCNP@lipid at 794 and 480 nm were measured under excitation at 980 nm. The energy transfer upconversion process in Tm-doped UCNPs involves a plethora of (de)population processes for each of the thulium excited states,[76] the precise intricacies of which are beyond the scope of this work. Thus, we limited ourselves to extracting the apparent decay lifetime from the data, using a monoexponential decay function. As expected, no significant differences in lifetime were observed for the 794 nm emission band (Figure 6A), since $[\mathbf{2}]^{2+}$ did not absorb light at

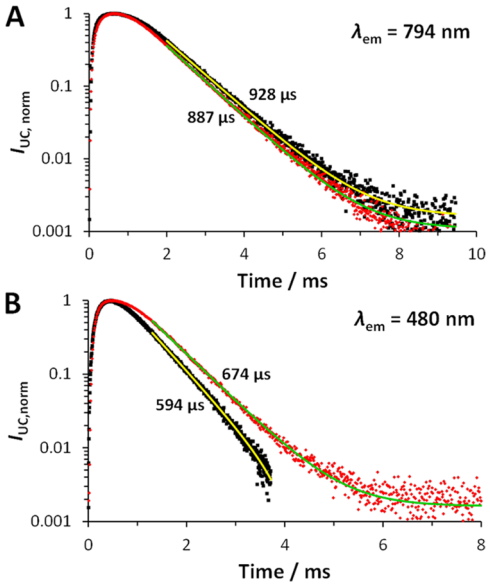

Figure 6. Logarithmic plot of the time-resolved emission of the Tm^{3+} emission bands at (A) 794 nm and (B) 480 nm for UCNP@lipid/[2] (black squares) and UCNP@lipid (red diamonds) under 980 nm excitation. Spectra were fitted using monoexponential decay functions (yellow for UCNP@lipid/[2] and green for UCNP@lipid) to determine the lifetimes of the Tm^{3+} states involved. UCNP composition: $NaYF_4$:Yb^{3+},Tm^{3+} (18, 0.3%).

this wavelength, and the lifetimes found were comparable to those reported in the literature.[77] However, the introduction of $[\mathbf{2}]^{2+}$ did result in a small reduction of the lifetime of the 480 nm emission band (Figure 6B), which was attributed to the occurrence of nonradiative Förster resonance energy transfer (FRET) to the ruthenium complex, with a FRET efficiency of 12%.

Regarding the fact that the UCNP emission band at 475 nm has been reduced by 20% upon introduction of the ruthenium complex (Figure 5B), we speculate that radiative energy transfer, or reabsorption, could also play a role in the sensitization of acceptor $[\mathbf{2}]^{2+}$ by the Tm^{3+} donor ions. The low FRET efficiency of 12% indicates that there is no efficient nonradiative energy transfer from the UCNP to $[\mathbf{2}]^{2+}$, either because the concentration of $[\mathbf{2}]^{2+}$ on the surface is too low or because the distance between the Tm^{3+} donors and the ruthenium acceptor is too large (≥5 nm). With respect to this distance, it is important to note that the strongest blue thulium emission stems from the center of the nanoparticles. This thulium ion is up to 26 nm away from the ruthenium ion, a distance far too great for FRET to take place, and so, energy transfer from the center of the UCNP fully relies on the radiative mechanism. The thulium ions near the surface of the nanoparticle are closer to $[\mathbf{2}]^{2+}$ and thus theoretically able to perform FRET. However, due to the lipid bilayer coating, the distance is not likely to become less than 4 nm, and the energy transfer to ruthenium is in competition with radiative decay, explaining the relatively low FRET efficiency found.

ROS Generation by UCNP@lipid/[2] under NIR Irradiation. The direct detection of the generation of singlet oxygen, by its phosphorescence at 1275 nm, is cumbersome in aqueous media as a result of the short lifetime (~3 µs) of singlet oxygen in water.[78] Thus, the detection of the amount of reactive oxygen species (ROS) generated by UCNP@lipid/[2] in MES buffer under NIR irradiation was performed by other means, i.e., using a chemical probe. The widely used 2′,7′-dichlorodihydrofluorescein ($DCFH_2^-$) probe was selected because it is very sensitive to a broad range of reactive oxygen species and well soluble in aqueous media.[79] Under the influence of ROS, the colorless $DCFH_2^-$ is oxidized to 2′,7′-dichlorofluorescein (DCF^{2-}), a dye with a strong absorbance at 502 nm (Scheme S5),[80] which allows for easy detection during the irradiation experiment by UV−vis absorption spectroscopy.

When UCNP@lipid/[2] was irradiated with 969 nm light in the presence of $DCFH_2^-$, a new absorption band emerged around 502 nm (Figure 7A), which was attributed to the formation of DCF^{2-}. Over 2 h of irradiation, the concentration of DCF^{2-} increased to 5.1 ± 2.5 µM, corresponding to the generation of 5.1 nmol of DCF^{2-} (Figure 7B). Although some formation of DCF^{2-} was also observed in the absence of the ruthenium complex, i.e., upon irradiation of UCNP@lipid ($[DCF^{2-}]_{final}$ = 1.1 ± 0.7 µM), this concentration was not significantly higher than the dark background signal (0.4 ± 0.4 µM). Thus, the activation of photosensitizer $[\mathbf{2}]^{2+}$ can clearly be achieved using the upconverted blue emission from Tm-doped UCNPs irradiated with NIR light. Subsequently, the amount of ROS generated under NIR irradiation was compared with the amount generated upon direct excitation of the ruthenium photosensitizer using blue light (Figure 8A). As expected, irradiation of UCNP@lipid/[2] with a blue laser resulted in the efficient generation of ROS, as judged by the very swift oxidation of the $DCFH_2^-$ to DCF^{2-}. Under the conditions used, all the $DCFH_2^-$ in the sample was oxidized within 15 min. However, irradiation of UCNP@lipid with blue light also led to the formation of DCF^{2-} (Figure 8A, black squares), albeit less efficiently than with UCNP@lipid/[2]. This is caused by the blue-light auto-oxidation of $DCFH_2^-$, indicated by the exponential increase of the DCF^{2-} concentration. More correctly, the oxidation of $DCFH_2^-$ is oxidized directly by an excited state $[DCF^{2-}]^*$ molecule, which itself was found to be a reasonably efficient photosensitizer (Φ_Δ = 0.08 in D_2O).[81,82] All in all, the blue-light sensitivity of $DCFH_2^-$ makes it difficult to compare the efficacy of UCNP@lipid/[2] under NIR and blue light.

DOI: 10.1021/acs.langmuir.9b01318
Langmuir 2019, 35, 12079−12090

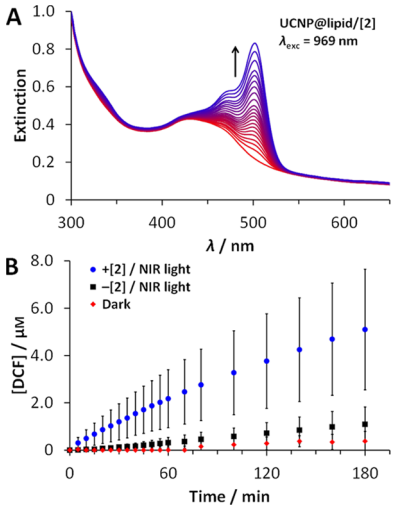

Figure 7. (A) Evolution of the UV−vis absorption spectra of a dispersion of UCNP@lipid/[**2**] containing $DCFH_2^-$ (10 μM) in aerated MES buffer ([UCNP] = 1.0 mg mL^{-1}, T = 25 °C) upon irradiation with a 969 nm CW laser beam (2.0 W, 50 W cm^{-2}) for 180 min. (B) Concentration of generated 2′,7′-dichlorofluorescein (DCF^{2-}, ε_{502} = 75 000 M^{-1} cm^{-1}) over time upon irradiation (969 nm, 2.0 W, 50 W cm^{-2}) of a dispersion of UCNP@lipid/[**2**] (blue circles) or UCNP@lipid (black squares) in MES buffer containing $DCFH_2^-$ (10 μM). Red diamonds indicate the dark control sample. The concentration of DCF^{2-} was determined from its absorbance at 502 nm.

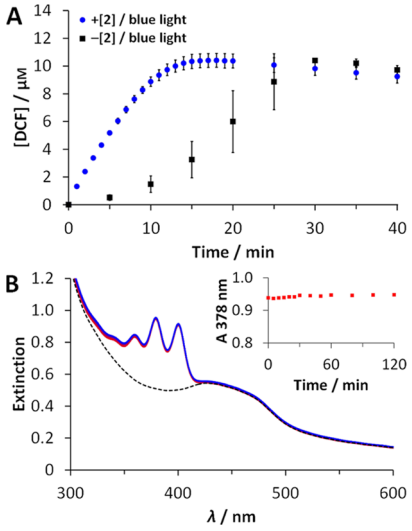

Figure 8. (A) Concentration of generated 2′,7′-dichlorofluorescein (DCF^{2-}) over time upon blue-light irradiation (450 nm, 50 mW, 0.40 W cm^{-2}) of a dispersion of UCNP@lipid/[**2**] (blue circles) or UCNP@lipid (black squares) in MES buffer containing $DCFH_2^-$ ([$DCFH_2^-$] = 10 μM, [UCNP] = 1.0 mg mL^{-1}, T = 25 °C). The concentration of DCF^{2-} was determined from its absorbance at 502 nm (ε_{502} = 75 000 M^{-1} cm^{-1}). (B) Evolution of the UV−vis absorption spectra of a dispersion of UCNP@lipid/[**2**] containing $ADMBMA^{4-}$ (50 μM) in aerated MES buffer ([UCNP] = 1.0 mg mL^{-1}, T = 25 °C) upon irradiation with a 969 nm CW laser beam (2.0 W, 50 W cm^{-2}) for 120 min. The dashed line represents the UV−vis absorption spectrum of UCNP@lipid/[**2**] prior to addition of the $ADMBMA^{4-}$ probe.

Besides its blue-light sensitivity, $DCFH_2^-$ is also known to be sensitive to most forms of reactive oxygen species, thus providing us with little information on the type of ROS generated by UCNP@lipid/[**2**].[79] Complex [**2**]$(PF_6)_2$ had already been shown to be a good singlet oxygen photosensitizer (Figure S5B). We therefore used one of the very few water-soluble $^1O_2$-specific probes available, tetrasodium 9,10-anthracenediyl-bis(methylene)-dimalonate (Na_4(ADMBMA)). This anthracene-based dye, absorbing light at around 378 nm, forms an endoperoxide in the presence of $^1O_2$, leading to a loss of conjugation and thus a decrease in its absorbance at 378 nm. In our case, no decrease in the absorbance of the $ADMBMA^{4-}$ probe could be observed when it was added to UCNP@lipid/[**2**] and the mixture was irradiated with NIR light. Although the most straightforward explanation for this observation is that UCNP@lipid/[**2**] does not produce $^1O_2$, but another form of ROS, another interpretation of this observation is that the strongly negatively charged $ADMBMA^{4-}$ probe may be electrostatically repelled by the negative surface charge of the UCNP@lipid/[**2**] nanoconjugate, keeping it too far away from the UCNP surface to react with the short-lived singlet oxygen produced there. Although it is also negatively charged, the ability of $DCFH_2^-$ to react with a wide range of ROS allows it to react with the more persistent secondary ROS generated from singlet oxygen, and its oxidation is thus less dependent on its distance from the nanoparticle surface. The cholesterol present in the lipid membrane could possibly play a role here as $^1O_2$ is known to be able to oxidize it, forming cholesterol hydroperoxides that could thereafter oxidize $DCFH_2^-$.[83] Some reports have even suggested that $DCFH_2^-$ is not at all oxidized by $^1O_2$ and that all formation of $DCF^{2-}$is caused by other (secondary) ROS.[81,82] In conclusion, despite being a non-selective probe for ROS, $DCFH_2^-$ was the only probe available that is capable of showing the formation of ROS with negatively charged lipid-coated UCNP nanoconjugates. Although a more selective, positively charged molecular probe would be desired to assess the type of ROS produced near the bilayer coating, there is no doubt that the irradiation of UCNP@lipid/[**2**] with NIR light generates a significant amount of ROS, and that the presence of ruthenium complex $[\mathbf{2}]^{2+}$ was essential for this ROS production.

CONCLUSIONS

In this work, we have shown that the exchange of one of the bpy ligands in $[Ru(bpy)_3]^{2+}$-type complexes by a 5,6-alkylether-modified phen ligand, as done in [**2**]$(PF_6)_2$, does not significantly alter the UV−vis absorption spectrum, nor does it reduce the phosphorescence or singlet oxygen generation quantum yield of complex [**2**]$(PF_6)_2$ when compared to $[Ru(bpy)_3]Cl_2$. However, the exchange of the bpy scaffold for the phen scaffold in the sterically strained complex [**1**]$(PF_6)_2$ does have serious implications for the selectivity and efficiency of its photosubstitution reaction, as it results in the nonselective expulsion of one of the three bidentate ligands and a low photosubstitution quantum yield. Unfortunately, this effect makes complex [**1**]$(PF_6)_2$ unsuited for PACT in a nanoparticle-based application.

On the other hand, the synthesis of the UCNP@lipid/[**2**] nanoconjugate shows that it is possible to use phospholipid coating for the functionalization of UCNPs with ruthenium complexes such as $[\mathbf{2}]^{2+}$. A stable, water-dispersible nanoconjugate free of excess lipids was obtained by two centrifugal washing steps. Energy transfer from the excited-state Tm^{3+} ions to the ruthenium complex was observed, although the efficiency was rather low. Potential causes of the limited

DOI: 10.1021/acs.langmuir.9b01318
Langmuir 2019, 35, 12079−12090

energy transfer efficiency may be found in the relatively large distance between the two components (5−26 nm), which strongly limits FRET efficiency, even when the spectral overlap between the upconverted emission of the UCNP and the absorption of the ruthenium complex is excellent. Recent work by Muhr et al. suggests that a reduction of the particle size to ∼20 nm could dramatically increase the FRET efficiency.[84] Another question is related to the supramolecular nature of the surface coating, which does not fully shield the UCNP surface from undesired quenchers, such as water. Protection of the UCNP surface from these quenchers is possible with the help of an undoped $NaYF_4$ shell layer on the outside of the particle,[60] but this comes at the price of a further increase in the distance between the Tm^{3+} and Ru^{2+} ions.

Despite the low efficiency of energy transfer, which limits the applicability of nanoconjugate UCNP@lipid/[**2**] in vivo, it has shown to produce measurable quantities of ROS under irradiation with a 969 nm laser, making it the first example of a ruthenium-based UCNP system for PDT. Determination of the type of ROS produced by the nanoparticle system was severely hindered by the lack of neutral or positively charged, water-soluble, chemical probes for the selective detection of ROS. The $ADMBMA^{4-}$ probe is too negatively charged to approach the negatively charged surface of the lipid bilayer of UCNP@lipid/[**2**] and thus not able to detect any of the short-lived singlet oxygen that may be produced at this surface. On the other hand, the $DCFH_2^-$ probe, the oxidation of which clearly indicates that the production of ROS by UCNP@lipid/[**2**] does occur, is not selective toward a specific type of ROS and most likely reacts with secondary ROS that has a longer lifetime than $^1O_2$. Singlet oxygen sensitizer green is a relatively novel commercial probe for the selective detection of $^1O_2$, but it is too negatively charged and suffers from its own issues with regard to photostability and light-induced self-activation.[85] Overall, the development of a selective, water-soluble probe for reactive oxygen species remains an open research challenge, not just in the field of nanoscience but also in the field of cell biology.

■ ASSOCIATED CONTENT

Supporting Information

The Supporting Information is available free of charge on the ACS Publications website at DOI: 10.1021/acs.langmuir.9b01318.

Ligand synthesis, ruthenium complex synthesis, UCNP synthesis and nanoparticle lipid encapsulation; details and spectra of nanoparticle characterization by XRD, TGA, (cryo-)TEM, ICP-OES, DLS, and ζ-potential measurements; spectroscopic details for quantum yield measurements (for photosubstitution, singlet oxygen generation, phosphorescence, and photon upconversion), upconversion luminescence, ROS-generation experiments, and nanosecond time-resolved emission spectroscopy; dark and light stability measurements of ruthenium complexes; NMR spectra (PDF)

■ AUTHOR INFORMATION

Corresponding Authors

*E-mail: martamaria.natile@unipd.it (M.M.N.).
*E-mail: bonnet@chem.leidenuniv.nl (S.B.).

ORCID

Michael S. Meijer: 0000-0003-0877-2374
Roxanne E. Kieltyka: 0000-0001-9152-1810
Albert M. Brouwer: 0000-0002-1731-3869
Marta M. Natile: 0000-0001-5591-2670
Sylvestre Bonnet: 0000-0002-5810-3657

Notes

The authors declare no competing financial interest.

■ ACKNOWLEDGMENTS

COST project CM1403: The European Upconversion Network is thanked for stimulating scientific discussion and for granting two short-term scientific missions to M.S.M. The European Research Council is acknowledged for a Starting grant to S.B. The Holland Research School for Molecular Chemistry (HRSMC) is thanked for a Fellowship to M.M.N. The National Research Council (Italy, CNR) is thanked for an STM-Fellowship to M.M.N. Dr. F. Boldrin and Dr. F. Caicci (Dept. of Biology, University of Padova) are thanked for producing TEM images. Dr. T. H. Sharp, Dr. R. I. Koning, and Prof. A. J. Koster (all Leiden University Medical Center) are acknowledged for support in performing the cryo-TEM imaging and access to the microscope. S.B. and M.S.M. kindly acknowledge Prof. E. Bouwman (Leiden University) for scientific discussion and support. M.M.N. kindly acknowledges Prof. L. Armelao (University of Padova) for scientific support.

■ REFERENCES

(1) Farrer, N. J.; Salassa, L.; Sadler, P. J. Photoactivated chemotherapy (PACT): the potential of excited-state d-block metals in medicine. *Dalton Trans.* **2009**, 10690−10701.

(2) Velema, W. A.; Szymanski, W.; Feringa, B. L. Photopharmacology: Beyond Proof of Principle. *J. Am. Chem. Soc.* **2014**, *136*, 2178−2191.

(3) Bonnet, S. Why develop photoactivated chemotherapy? *Dalton Trans.* **2018**, *47*, 10330−10343.

(4) Gai, S.; Yang, G.; Yang, P.; He, F.; Lin, J.; Jin, D.; Xing, B. Recent advances in functional nanomaterials for light−triggered cancer therapy. *Nano Today* **2018**, *19*, 146−187.

(5) Mari, C.; Pierroz, V.; Ferrari, S.; Gasser, G. Combination of Ru(ii) complexes and light: new frontiers in cancer therapy. *Chem. Sci.* **2015**, *6*, 2660−2686.

(6) Cloonan, S. M.; Elmes, R.; Erby, M.; Bright, S. A.; Poynton, F. E.; Nolan, D. E.; Quinn, S. J.; Gunnlaugsson, T.; Williams, D. C. Detailed Biological Profiling of a Photoactivated and Apoptosis Inducing pdppz Ruthenium (II) Polypyridyl complex in Cancer Cells. *J. Med. Chem.* **2015**, *58*, 4494−4505.

(7) Garner, R. N.; Gallucci, J. C.; Dunbar, K. R.; Turro, C. [Ru(bpy)2(5-cyanouracil)2]2+ as a Potential Light-Activated Dual-Action Therapeutic Agent. *Inorg. Chem.* **2011**, *50*, 9213−9215.

(8) Zayat, L.; Calero, C.; Alborés, P.; Baraldo, L.; Etchenique, R. A New Strategy for Neurochemical Photodelivery: Metal−Ligand Heterolytic Cleavage. *J. Am. Chem. Soc.* **2003**, *125*, 882−883.

(9) Frasconi, M.; Liu, Z.; Lei, J.; Wu, Y.; Strekalova, E.; Malin, D.; Ambrogio, M. W.; Chen, X.; Botros, Y. Y.; Cryns, V. L.; Sauvage, J.-P.; Stoddart, J. F. Photoexpulsion of Surface-Grafted Ruthenium Complexes and Subsequent Release of Cytotoxic Cargos to Cancer Cells from Mesoporous Silica Nanoparticles. *J. Am. Chem. Soc.* **2013**, *135*, 11603−11613.

(10) Shi, G.; Monro, S.; Hennigar, R.; Colpitts, J.; Fong, J.; Kasimova, K.; Yin, H.; DeCoste, R.; Spencer, C.; Chamberlain, L.; Mandel, A.; Lilge, L.; McFarland, S. A. Ru(II) dyads derived from α-oligothiophenes: A new class of potent and versatile photosensitizers for PDT. *Coord. Chem. Rev.* **2015**, *282*−*283*, 127−138.

(11) Hess, J.; Huang, H.; Kaiser, A.; Pierroz, V.; Blacque, O.; Chao, H.; Gasser, G. Evaluation of the Medicinal Potential of Two Ruthenium(II) Polypyridine Complexes as One- and Two-Photon

DOI: 10.1021/acs.langmuir.9b01318
Langmuir 2019, 35, 12079−12090

Photodynamic Therapy Photosensitizers. *Chem. - Eur. J.* **2017**, *23*, 9888−9896.
(12) van Rixel, V. H. S.; Siewert, B.; Hopkins, S. L.; Askes, S. H. C.; Busemann, A.; Siegler, M. A.; Bonnet, S. Green light-induced apoptosis in cancer cells by a tetrapyridyl ruthenium prodrug offering two trans coordination sites. *Chem. Sci.* **2016**, *7*, 4922−4929.
(13) Hidayatullah, A. N.; Wachter, E.; Heidary, D. K.; Parkin, S.; Glazer, E. C. Photoactive Ru(II) Complexes With Dioxinophenanthroline Ligands Are Potent Cytotoxic Agents. *Inorg. Chem.* **2014**, *53*, 10030−10032.
(14) Zamora, A.; Denning, C. A.; Heidary, D. K.; Wachter, E.; Nease, L. A.; Ruiz, J.; Glazer, E. C. Ruthenium-containing P450 inhibitors for dual enzyme inhibition and DNA damage. *Dalton Trans.* **2017**, *46*, 2165−2173.
(15) Heinemann, F.; Karges, J.; Gasser, G. Critical Overview of the Use of Ru(II) Polypyridyl Complexes as Photosensitizers in One-Photon and Two-Photon Photodynamic Therapy. *Acc. Chem. Res.* **2017**, *50*, 2727−2736.
(16) Karaoun, N.; Renfrew, A. K. A luminescent ruthenium(ii) complex for light-triggered drug release and live cell imaging. *Chem. Commun.* **2015**, *51*, 14038−14041.
(17) Lameijer, L. N.; Ernst, D.; Hopkins, S. L.; Meijer, M. S.; Askes, S. H. C.; Le Dévédec, S. E.; Bonnet, S. A red light-activated ruthenium-caged NAMPT inhibitor remains phototoxic in hypoxic cancer cells. *Angew. Chem., Int. Ed.* **2017**, *56*, 11549−11553.
(18) Li, A.; Yadav, R.; White, J. K.; Herroon, M. K.; Callahan, B. P.; Podgorski, I.; Turro, C.; Scott, E. E.; Kodanko, J. J. Illuminating cytochrome P450 binding: Ru(ii)-caged inhibitors of CYP17A1. *Chem. Commun.* **2017**, *53*, 3673−3676.
(19) Laemmel, A.-C.; Collin, J.-P.; Sauvage, J.-P. Efficient and Selective Photochemical Labilization of a Given Bidentate Ligand in Mixed Ruthenium(II) Complexes of the Ru(phen)2L2+ and Ru(bipy)2L2+ Family (L = Sterically Hindering Chelate). *Eur. J. Inorg. Chem.* **1999**, *1999*, 383−386.
(20) Sun, Q.; Mosquera-Vazquez, S.; Lawson Daku, L. M.; Guénée, L.; Goodwin, H. A.; Vauthey, E.; Hauser, A. Experimental Evidence of Ultrafast Quenching of the 3MLCT Luminescence in Ruthenium(II) Tris-bipyridyl Complexes via a 3dd State. *J. Am. Chem. Soc.* **2013**, *135*, 13660−13663.
(21) Wachter, E.; Heidary, D. K.; Howerton, B. S.; Parkin, S.; Glazer, E. C. Light-activated ruthenium complexes photobind DNA and are cytotoxic in the photodynamic therapy window. *Chem. Commun.* **2012**, *48*, 9649−9651.
(22) Howerton, B. S.; Heidary, D. K.; Glazer, E. C. Strained Ruthenium Complexes Are Potent Light-Activated Anticancer Agents. *J. Am. Chem. Soc.* **2012**, *134*, 8324−8327.
(23) Bonnet, S.; Collin, J. P.; Sauvage, J. P.; Schofield, E. Photochemical Expulsion of the Neutral Monodentate Ligand L in Ru(terpy*)(diimine)(L)(2+): A Dramatic Effect of the Steric Properties of the Spectator Diimine Ligand. *Inorg. Chem.* **2004**, *43*, 8346−8354.
(24) Hopkins, S. L.; Siewert, B.; Askes, S. H. C.; Veldhuizen, P.; Zwier, R.; Heger, M.; Bonnet, S. An in vitro cell irradiation protocol for testing photopharmaceuticals and the effect of blue, green, and red light on human cancer cell lines. *Photochem. Photobiol. Sci.* **2016**, *15*, 644−653.
(25) Bashkatov, A. N.; Genina, E. A.; Kochubey, V. I.; Tuchin, V. V. Optical properties of human skin, subcutaneous and mucous tissues in the wavelength range from 400 to 2000 nm. *J. Phys. D: Appl. Phys.* **2005**, *38*, 2543−2555.
(26) Askes, S. H. C.; Meijer, M. S.; Bouwens, T.; Landman, I.; Bonnet, S. Red Light Activation of Ru(II) Polypyridyl Prodrugs via Triplet-Triplet Annihilation Upconversion: Feasibility in Air and through Meat. *Molecules* **2016**, *21*, 1460.
(27) Gorris, H. H.; Resch-Genger, U. Perspectives and Challenges of Photon-upconversion Nanoparticles − Part II: Bioanalytical Applications. *Anal. Bioanal. Chem.* **2017**, *409*, 5875−5890.
(28) Liu, X.; Chen, H.-C.; Kong, X.; Zhang, Y.; Tu, L.; Chang, Y.; Wu, F.; Wang, T.; Reek, J. N. H.; Brouwer, A. M.; Zhang, H. Near infrared light-driven water oxidation in a molecule-based artificial photosynthetic device using an upconversion nano-photosensitizer. *Chem. Commun.* **2015**, *51*, 13008−13011.
(29) Tang, Y.; Di, W.; Zhai, X.; Yang, R.; Qin, W. NIR-Responsive Photocatalytic Activity and Mechanism of $NaYF_4$:Yb,Tm@TiO_2 Core−Shell Nanoparticles. *ACS Catal.* **2013**, *3*, 405−412.
(30) Xu, Z.; Quintanilla, M.; Vetrone, F.; Govorov, A. O.; Chaker, M.; Ma, D. Harvesting Lost Photons: Plasmon and Upconversion Enhanced Broadband Photocatalytic Activity in Core@Shell Microspheres Based on Lanthanide-Doped $NaYF_4$, TiO_2, and Au. *Adv. Funct. Mater.* **2015**, *25*, 2950−2960.
(31) Bagheri, A.; Arandiyan, H.; Boyer, C.; Lim, M. Lanthanide-Doped Upconversion Nanoparticles: Emerging Intelligent Light-Activated Drug Delivery Systems. *Adv. Sci.* **2016**, *3*, No. 1500437.
(32) Deng, K.; Li, C.; Huang, S.; Xing, B.; Jin, D.; Zeng, Q.; Hou, Z.; Lin, J. Recent Progress in Near Infrared Light Triggered Photodynamic Therapy. *Small* **2017**, *13*, No. 1702299.
(33) Ruggiero, E.; Alonso-de Castro, S.; Habtemariam, A.; Salassa, L. Upconverting Nanoparticles for the Near-infrared Photoactivation of Transition Metal Complexes: New Opportunities and Challenges in Medicinal Inorganic Photochemistry. *Dalton Trans.* **2016**, *45*, 13012−13020.
(34) Wang, D.; Xue, B.; Kong, X.; Langping, T.; Liu, X.; Zhang, Y.; Chang, Y.; Luo, Y.; Zhao, H.; Zhang, H. 808 nm Driven Nd3+-Sensitized Upconversion Nanostructures for Photodynamic Therapy and Simultaneous Fluorescence Imaging. *Nanoscale* **2015**, *7*, 190−197.
(35) Chen, Z.; Thiramanas, R.; Schwendy, M.; Xie, C.; Parekh, S. H.; Mailänder, V.; Wu, S. Upconversion Nanocarriers Encapsulated with Photoactivatable Ru Complexes for Near-Infrared Light-Regulated Enzyme Activity. *Small* **2017**, *13*, No. 1700997.
(36) Yu, Q.; Rodriguez, E. M.; Naccache, R.; Forgione, P.; Lamoureux, G.; Sanz-Rodriguez, F.; Scheglmann, D.; Capobianco, J. A. Chemical modification of temoporfin - a second generation photosensitizer activated using upconverting nanoparticles for singlet oxygen generation. *Chem. Commun.* **2014**, *50*, 12150−12153.
(37) Pierri, A. E.; Huang, P.-J.; Garcia, J. V.; Stanfill, J. G.; Chui, M.; Wu, G.; Zheng, N.; Ford, P. C. A photoCORM nanocarrier for CO release using NIR light. *Chem. Commun.* **2015**, *51*, 2072−2075.
(38) Näreoja, T.; Deguchi, T.; Christ, S.; Peltomaa, R.; Prabhakar, N.; Fazeli, E.; Perälä, N.; Rosenholm, J. M.; Arppe, R.; Soukka, T.; Schäferling, M. Ratiometric Sensing and Imaging of Intracellular pH Using Polyethylenimine-Coated Photon Upconversion Nanoprobes. *Anal. Chem.* **2017**, *89*, 1501−1508.
(39) Mattsson, L.; Wegner, K. D.; Hildebrandt, N.; Soukka, T. Upconverting nanoparticle to quantum dot FRET for homogeneous double-nano biosensors. *RSC Adv.* **2015**, *5*, 13270−13277.
(40) Drees, C.; Raj, A. N.; Kurre, R.; Busch, K. B.; Haase, M.; Piehler, J. Engineered Upconversion Nanoparticles for Resolving Protein Interactions inside Living Cells. *Angew. Chem., Int. Ed.* **2016**, *55*, 11668−11672.
(41) Kim, W. J.; Nyk, M.; Prasad, P. N. Color-coded Multilayer Photopatterned Microstructures using Lanthanide(III)-ion Co-doped $NaYF_4$ Nanoparticles with Upconversion Luminescence for Possible Applications in Security. *Nanotechnology* **2009**, *20*, No. 185301.
(42) Resch-Genger, U.; Gorris, H. H. Perspectives and challenges of photon-upconversion nanoparticles—part I: routes to brighter particles and quantitative spectroscopic studies. *Anal. Bioanal. Chem.* **2017**, *409*, 5855−5874.
(43) Hamblin, M. R. Upconversion in photodynamic therapy: plumbing the depths. *Dalton Trans.* **2018**, *47*, 8571−8580.
(44) Wang, C.; Cheng, L.; Liu, Z. Upconversion Nanoparticles for Photodynamic Therapy and Other Cancer Therapeutics. *Theranostics* **2013**, *3*, 317−330.
(45) He, S.; Johnson, N. J. J.; Nguyen Huu, V. A.; Huang, Y.; Almutairi, A. Leveraging Spectral Matching between Photosensitizers and Upconversion Nanoparticles for 808 nm-Activated Photodynamic Therapy. *Chem. Mater.* **2018**, *30*, 3991−4000.

DOI: 10.1021/acs.langmuir.9b01318
Langmuir 2019, 35, 12079−12090

(46) Chen, X. L.; Zhao, Z. X.; Jiang, M. Y.; Que, D. P.; Shi, S. G.; Zheng, N. F. Preparation and Photodynamic Therapy Application of NaYF4:Yb,Tm-NaYF4:Yb,Er Multifunctional Upconverting Nanoparticles. *New J. Chem.* **2013**, *37*, 1782−1788.
(47) Sabri, T.; Pawelek, P.; Capobianco, J. A. Dual Activity of Rose Bengal Functionalized to Albumin-Coated Lanthanide-Doped Upconverting Nanoparticles: Targeting and Photodynamic Therapy. *ACS Appl. Mater. Interfaces* **2018**, *10*, 26947−26953.
(48) Liu, X.; Zheng, M.; Kong, X.; Zhang, Y.; Zeng, Q.; Sun, Z.; Buma, W. J.; Zhang, H. Separately doped upconversion-C60 nanoplatform for NIR imaging-guided photodynamic therapy of cancer cells. *Chem. Commun.* **2013**, *49*, 3224−3226.
(49) Khaydukov, E. V.; Mironova, K. E.; Semchishen, V. A.; Generalova, A. N.; Nechaev, A. V.; Khochenkov, D. A.; Stepanova, E. V.; Lebedev, O. I.; Zvyagin, A. V.; Deyev, S. M.; Panchenko, V. Y. Riboflavin photoactivation by upconversion nanoparticles for cancer treatment. *Sci. Rep.* **2016**, *6*, No. 35103.
(50) Ruggiero, E.; Habtemariam, A.; Yate, L.; Mareque-Rivas, J. C.; Salassa, L. Near infrared photolysis of a Ru polypyridyl complex by upconverting nanoparticles. *Chem. Commun.* **2014**, *50*, 1715−1718.
(51) Ruggiero, E.; Garino, C.; Mareque-Rivas, J. C.; Habtemariam, A.; Salassa, L. Upconverting Nanoparticles Prompt Remote Near-Infrared Photoactivation of Ru(II)−Arene Complexes. *Chem. - Eur. J.* **2016**, *22*, 2801−2811.
(52) He, S.; Krippes, K.; Ritz, S.; Chen, Z.; Best, A.; Butt, H.-J.; Mailander, V.; Wu, S. Ultralow-intensity near-infrared light induces drug delivery by upconverting nanoparticles. *Chem. Commun.* **2015**, *51*, 431−434.
(53) Xiang, H.-J.; Deng, Q.; An, L.; Guo, M.; Yang, S.-P.; Liu, J.-G. Tumor cell specific and lysosome-targeted delivery of nitric oxide for enhanced photodynamic therapy triggered by 808 nm near-infrared light. *Chem. Commun.* **2016**, *52*, 148−151.
(54) Zhang, Y.; Yu, Z.; Li, J.; Ao, Y.; Xue, J.; Zeng, Z.; Yang, X.; Tan, T. T. Y. Ultrasmall-Superbright Neodymium-Upconversion Nanoparticles via Energy Migration Manipulation and Lattice Modification: 808 nm-Activated Drug Release. *ACS Nano* **2017**, *11*, 2846−2857.
(55) Wilhelm, S.; Kaiser, M.; Würth, C.; Heiland, J.; Carrillo-Carrion, C.; Muhr, V.; Wolfbeis, O. S.; Parak, W. J.; Resch-Genger, U.; Hirsch, T. Water dispersible upconverting nanoparticles: effects of surface modification on their luminescence and colloidal stability. *Nanoscale* **2015**, *7*, 1403−1410.
(56) Rojas-Gutierrez, P. A.; DeWolf, C.; Capobianco, J. A. Formation of a Supported Lipid Bilayer on Faceted $LiYF_4$:Tm^{3+}/Yb^{3+} Upconversion Nanoparticles. *Part. Part. Syst. Charact.* **2016**, *33*, 865−870.
(57) Ruggiero, E.; Hernandez-Gil, J.; Mareque Rivas, J.; Salassa, L. Near Infrared Activation of an Anticancer PtIV Complex by Tm-Doped Upconverting Nanoparticles. *Chem. Commun.* **2015**, *51*, 2091−2094.
(58) Rojas-Gutierrez, P. A.; Bhuckory, S.; Mingoes, C.; Hildebrandt, N.; DeWolf, C. E.; Capobianco, J. A. A Route to Triggered Delivery via Photocontrol of Lipid Bilayer Properties Using Lanthanide Upconversion Nanoparticles. *ACS Appl. Nano Mater.* **2018**, *1*, 5345−5354.
(59) Wang, H. J.; Shrestha, R.; Zhang, Y. Encapsulation of Photosensitizers and Upconversion Nanocrystals in Lipid Micelles for Photodynamic Therapy. *Part. Part. Syst. Charact.* **2014**, *31*, 228−235.
(60) Ding, Y.; Wu, F.; Zhang, Y.; Liu, X.; de Jong, E. M. L. D.; Gregorkiewicz, T.; Hong, X.; Liu, Y.; Aalders, M. C. G.; Buma, W. J.; Zhang, H. Interplay between Static and Dynamic Energy Transfer in Biofunctional Upconversion Nanoplatforms. *J. Phys. Chem. Lett.* **2015**, *6*, 2518−2523.
(61) Garcìa-Fresnadillo, D.; Georgiadou, Y.; Orellana, G.; Braun, A. M.; Oliveros, E. Singlet-Oxygen (1Δg) Production by Ruthenium(II) complexes containing polyazaheterocyclic ligands in methanol and in water. *Helv. Chim. Acta* **1996**, *79*, 1222−1238.
(62) Liu, Q.; Feng, W.; Yang, T.; Yi, T.; Li, F. Upconversion luminescence imaging of cells and small animals. *Nat. Protoc.* **2013**, *8*, 2033−2044.
(63) Bergström, L.; Shinozaki, K.; Tomiyama, H.; Mizutani, N. Colloidal Processing of a Very Fine BaTiO3 Powder — Effect of Particle Interactions on the Suspension Properties, Consolidation, and Sintering Behavior. *J. Am. Ceram. Soc.* **1997**, *80*, 291−300.
(64) Suyver, J. F.; Aebischer, A.; García-Revilla, S.; Gerner, P.; Güdel, H. U. Anomalous power dependence of sensitized upconversion luminescence. *Phys. Rev. B* **2005**, *71*, No. 125123.
(65) Pollnau, M.; Gamelin, D. R.; Lüthi, S. R.; Güdel, H. U.; Hehlen, M. P. Power dependence of upconversion luminescence in lanthanide and transition-metal-ion systems. *Phys. Rev. B* **2000**, *61*, 3337−3346.
(66) Meijer, M. S.; Rojas-Gutierrez, P. A.; Busko, D.; Howard, I. A.; Frenzel, F.; Würth, C.; Resch-Genger, U.; Richards, B. S.; Turshatov, A.; Capobianco, J. A.; Bonnet, S. Absolute Upconversion Quantum Yields of Blue-emitting LiYF4:Yb3+,Tm3+ Upconverting Nanoparticles. *Phys. Chem. Chem. Phys.* **2018**, *20*, 22556−22562.
(67) Zheng, R. H.; Guo, H. C.; Jiang, H. J.; Xu, K. H.; Liu, B. B.; Sun, W. L.; Shen, Z. Q. A new and convenient synthesis of phendiones oxidated by KBrO3/H2SO4 at room temperature. *Chin. Chem. Lett.* **2010**, *21*, 1270−1272.
(68) Laemmel, A.-C.; Collin, J.-P.; Sauvage, J.-P.; Accorsi, G.; Armaroli, N. Macrocyclic Complexes of [Ru(N-N)2]2+ Units [N-N = 1,10 Phenanthroline or 4-(p-Anisyl)-1,10-Phenanthroline]: Synthesis and Photochemical Expulsion Studies. *Eur. J. Inorg. Chem.* **2003**, *2003*, 467−474.
(69) Kohler, L.; Nease, L.; Vo, P.; Garofolo, J.; Heidary, D. K.; Thummel, R. P.; Glazer, E. C. Photochemical and Photobiological Activity of Ru(II) Homoleptic and Heteroleptic Complexes Containing Methylated Bipyridyl-type Ligands. *Inorg. Chem.* **2017**, *56*, 12214−12223.
(70) Baranoff, E.; Collin, J.-P.; Furusho, J.; Furusho, Y.; Laemmel, A.-C.; Sauvage, J.-P. Photochemical or Thermal Chelate Exchange in the Ruthenium Coordination Sphere of Complexes of the Ru(phen)-2L Family (L = Diimine or Dinitrile Ligands). *Inorg. Chem.* **2002**, *41*, 1215−1222.
(71) Cuello-Garibo, J.-A.; Pérez-Gallent, E.; van der Boon, L.; Siegler, M. A.; Bonnet, S. Influence of the Steric Bulk and Solvent on the Photoreactivity of Ruthenium Polypyridyl Complexes Coordinated to l-Proline. *Inorg. Chem.* **2017**, *56*, 4818−4828.
(72) Alwarawrah, M.; Dai, J.; Huang, J. A Molecular View of the Cholesterol Condensing Effect in DOPC Lipid Bilayers. *J. Phys. Chem. B* **2010**, *114*, 7516−7523.
(73) Boyer, J.-C.; Manseau, M.-P.; Murray, J. I.; van Veggel, F. C. J. M. Surface Modification of Upconverting NaYF4 Nanoparticles with PEG-Phosphate Ligands for NIR (800 nm) Biolabeling within the Biological Window. *Langmuir* **2010**, *26*, 1157−1164.
(74) Cao, P.; Tong, L.; Hou, Y.; Zhao, G.; Guerin, G.; Winnik, M. A.; Nitz, M. Improving Lanthanide Nanocrystal Colloidal Stability in Competitive Aqueous Buffer Solutions using Multivalent PEG-Phosphonate Ligands. *Langmuir* **2012**, *28*, 12861−12870.
(75) Plohl, O.; Kraft, M.; Kovač, J.; Belec, B.; Ponikvar-Svet, M.; Würth, C.; Lisjak, D.; Resch-Genger, U. Optically Detected Degradation of NaYF4:Yb,Tm-Based Upconversion Nanoparticles in Phosphate Buffered Saline Solution. *Langmuir* **2017**, *33*, 553−560.
(76) Liu, G. Advances in the theoretical understanding of photon upconversion in rare-earth activated nanophosphors. *Chem. Soc. Rev.* **2015**, *44*, 1635−1652.
(77) Arppe, R.; Hyppanen, I.; Perala, N.; Peltomaa, R.; Kaiser, M.; Würth, C.; Christ, S.; Resch-Genger, U.; Schaferling, M.; Soukka, T. Quenching of the upconversion luminescence of NaYF4:Yb3+,Er3+ and NaYF4:Yb3+,Tm3+ nanophosphors by water: the role of the sensitizer Yb3+ in non-radiative relaxation. *Nanoscale* **2015**, *7*, 11746−11757.
(78) Egorov, S. Y.; Kamalov, V. F.; Koroteev, N. I.; Krasnovsky, A. A.; Toleutaev, B. N.; Zinukov, S. V. Rise and decay kinetics of photosensitized singlet oxygen luminescence in water. Measurements

DOI: 10.1021/acs.langmuir.9b01318
Langmuir 2019, 35, 12079−12090

with nanosecond time-correlated single photon counting technique. *Chem. Phys. Lett.* **1989**, *163*, 421−424.
(79) Wang, S. T.; Zhegalova, N. G.; Gustafson, T. P.; Zhou, A.; Sher, J.; Achilefu, S.; Berezin, O. Y.; Berezin, M. Y. Sensitivity of activatable reactive oxygen species probes by fluorescence spectroelectrochemistry. *Analyst* **2013**, *138*, 4363−4369.
(80) Taniguchi, M.; Lindsey, J. S. Database of Absorption and Fluorescence Spectra of >300 Common Compounds for use in PhotochemCAD. *Photochem. Photobiol.* **2018**, *94*, 290−327.
(81) Bilski, P.; Belanger, A. G.; Chignell, C. F. Photosensitized oxidation of 2′,7′-dichlorofluorescin: singlet oxygen does not contribute to the formation of fluorescent oxidation product 2′,7′-dichlorofluorescein. *Free Radical Biol. Med.* **2002**, *33*, 938−946.
(82) Chen, X.; Zhong, Z.; Xu, Z.; Chen, L.; Wang, Y. 2′,7′-Dichlorodihydrofluorescein as a fluorescent probe for reactive oxygen species measurement: Forty years of application and controversy. *Free Radical Res.* **2010**, *44*, 587−604.
(83) Murphy, R. C.; Johnson, K. M. Cholesterol, reactive oxygen species, and the formation of biologically active mediators. *J. Biol. Chem.* **2008**, *283*, 15521−15525.
(84) Muhr, V.; Würth, C.; Kraft, M.; Buchner, M.; Baeumner, A. J.; Resch-Genger, U.; Hirsch, T. Particle-Size-Dependent Förster Resonance Energy Transfer from Upconversion Nanoparticles to Organic Dyes. *Anal. Chem.* **2017**, *89*, 4868−4874.
(85) Kim, S.; Fujitsuka, M.; Majima, T. Photochemistry of Singlet Oxygen Sensor Green. *J. Phys. Chem. B* **2013**, *117*, 13985−13992.

DOI: 10.1021/acs.langmuir.9b01318
Langmuir 2019, 35, 12079−12090